Am J Cancer Res 2023;13(12):5914-5933
www.ajcr.us /ISSN:2156-6976/ajcr0148807

Original Article

Cancer cell seeding density as a mechanism of chemotherapy resistance: a novel cancer cell density index based on IC50-Seeding Density Slope (ISDS) to assess chemosensitivity

Ujwal Punyamurtula[1,2,8], Thomas W Brown[2,3], Shengliang Zhang[2,4,5,6], Andrew George[2,3,4], Wafik S El-Deiry[2,4,5,6,7]

[1]Biotechnology Graduate Program, Department of Molecular Pharmacology, Physiology and Biotechnology, Division of Biology and Medicine, Brown University, Providence, RI, USA; [2]Legorreta Cancer Center at Brown University, The Warren Alpert Medical School of Brown University, Providence, RI, USA; [3]Department of Molecular Biology, Cell Biology and Biochemistry, Division of Biology and Medicine, Brown University, Providence, RI, USA; [4]Laboratory of Translational Oncology and Experimental Cancer Therapeutics, The Warren Alpert Medical School of Brown University, Providence, RI, USA; [5]Department of Pathology and Laboratory Medicine, The Warren Alpert Medical School of Brown University, Providence, RI, USA; [6]Joint Program in Cancer Biology, Brown University and Lifespan Health System, Providence, RI, USA; [7]Division of Hematology/Oncology, The Warren Alpert Medical School of Brown University, Providence, RI, USA; [8]Department of Cancer Biology, Dana-Farber Cancer Institute, Boston, MA, USA

Received December 28, 2022; Accepted November 14, 2023; Epub December 15, 2023; Published December 30, 2023

Abstract: Although the 50% inhibitory concentration (IC50) is a commonly used measurement of chemosensitivity in cancer cells, it has been known to vary with the density of the treated cells (in that more densely seeded cells are more resistant to chemotherapeutic agents). Indeed, density-dependent chemoresistance may be a significant independent mechanism of therapy resistance. We examine the nature of cell density-dependent chemoresistance and explore possible underlying mechanisms. CellTiter-Glo assays and ethidium homodimer staining revealed that response to chemotherapy is density-dependent in all cancer cell lines tested. Our results prompted us to develop a novel cancer cell seeding density index of chemosensitivity, the ISDS (IC50-Seeding Density Slope), which we propose can serve as an improved method of analyzing how cancer cells respond to chemotherapeutic treatment compared to the widely-used IC50. Furthermore, western blot analysis suggests that levels of autophagy and apoptotic markers are modulated by cancer cell density. Cell viability experiments using the autophagy inhibitor chloroquine showed that chloroquine's efficacy was reduced at higher cell densities and that chloroquine and cisplatin exhibited synergy at both higher and lower cell densities in TOV-21G cells. We discuss alternative mechanisms of density-dependent chemoresistance and *in vivo*/clinical applications, including challenges of adjuvant chemotherapy and minimal residual disease. Taken together, our findings show that cell density is a significant contributor in shaping cancer chemosensitivity, that the ISDS (aka the Ujwal Punyamurtula/Wafik El-Deiry or Ujwal-WAF Index) can be used to effectively assess cell viability and that this phenomenon of density-dependent chemoresistance may be leveraged for a variety of biologic and cancer therapeutic applications.

Keywords: Seeding density, cell culture, chemotherapeutic resistance, cancer, cancer cell density index, cell seeding density index, IC50-Seeding Density Slope, ISDS

Introduction

Several clinical studies have shown that even though there may be a dramatic/significant initial response to a given treatment strategy, tumors are notorious in their ability to easily develop resistance to said treatment, and the development of this resistance can be influenced by a variety of factors [1]. This phenomenon of therapy resistance, especially in the context of chemotherapeutic small molecules, has only stressed the importance of pre-clinical

studies, not only for optimizing existing treatment strategies but also for unraveling mechanisms by which therapy resistance might develop and how it could be addressed.

However, assessing chemotherapeutic resistance in cancer cells has not been without its challenges. Measurements of the half-maximal inhibitory concentration (IC50), by far the most widely used evaluation of how cancer cells respond to chemotherapy *in vitro*, have tended to be inconsistent, and such inconsistencies have lent themselves to a wide variety of conflicting results in modern cancer research [2]. In their investigation of the limitations of the MTT *in vitro* assay for IC50 measurement, He *et al.* dissected the causes behind the assay's inconsistencies and found that these inconsistencies produced large and incorrigible errors in IC50 measurement [2].

Under the assumption that the observed density-dependent chemoresistance variations were due to the limitations of traditional cell-plating-based cell viability assays, He *et al.* developed a novel limiting dilution assay, which directly counted the cells following cisplatin treatment, in order to provide more precise and objective IC50 measurements. However, these authors found that the observed variations in density-dependent cisplatin resistance persisted, signifying that density-dependent chemoresistance may be an inherent property of cancer cells [2]. In support of this discovery, in several of our own preliminary experiments using the CellTiter-Glo assay for cell viability measurements, we consistently observed that tumor cells that were plated at higher densities consistently tended to be more resistant to chemotherapeutic agents.

Despite the findings previously reported, however, several questions are still left to be answered regarding density-dependent chemoresistance variation. For instance, how are levels of cell death modulated at various seeding densities? Can an *in vitro* assessment of cellular response to chemotherapy that takes density-dependent chemoresistance into account be developed? More importantly, what are the underlying mechanisms behind this commonly-observed phenomenon, and how can they be leveraged for *in vivo* and clinical applications [2, 3]? Evidently, there remains a need for further investigation into the nature of density-dependent chemoresistance. As a result, it is exigent to conduct experiments that not only further characterize density-dependent chemoresistance but also investigate various mechanisms by which such resistance variations can occur.

Methods

Cell lines

The majority of experiments presented in this study utilize the TOV-21G ovarian cancer cell line TOV-21G is a clear-cell ovarian carcinoma cell line. Although it contains WT p53, TOV-21G is characterized by numerous genetic alterations (*SIB Swiss Institute of Bioinformatics. Cellosaurus TOV-21G (CVCL_3613). https://www.cellosaurus.org/CVCL_3613)*, including mutations in *KRAS*, *PIK3CA*, and *PTEN* [4]. In addition, TOV-21G contains such abnormalities as significant microsatellite instability and a trisomy of chromosome 10 [4].

TOV-21G was chosen for the experiments reported in this study for numerous reasons, chief among them being the fact that it is an adherent cell line that grows quickly, making it convenient to use in cell culture assays. Moreover, various other ovarian cancer cell lines were used by He *et al.* in their detailed study of density-dependent chemoresistance, making TOV-21G a suitable starting point for the density-dependent experiments conducted in this project.

A second clear-cell ovarian carcinoma cell line, OVMANA, was also included to support the replicability of the study's findings within cancer types. OVMANA is WT for *TP53* and has elevated MDM2 expression [5]. This cell line also contains a mutation in *PIK3CA (SIB Swiss Institute of Bioinformatics. Cellosaurus OVMANA (CVCL_3111). https://www.cellosaurus.org/CVCL_3111)*. OVMANA is an adherent cell line that grows slower than TOV-21G.

Colorectal cell lines, SW-480 and HT-29, an osteosarcoma cell line, U-2 OS, and a pancreatic cell line, PANC1, were utilized to demonstrate study replicability across different cancer types. Both SW-480 and HT-29 have Arg-273His mutations in the *TP53* gene, resulting in p53 overexpression. SW-480 cells contain an additional Pro309Ser mutation in the *TP53*

gene, along with alterations in *KRAS* and *APC*. *APC, BRAF, PIK3CA*, and *SMAD4* mutations are also present in the HT-29 cell line (SIB Swiss Institute of Bioinformatics. Cellosaurus SW480 (CVCL_0546). https://www.cellosaurus.org/CVCL_0546; SIB Swiss Institute of Bioinformatics. Cellosaurus HT-29 (CVCL_0320). https://www.cellosaurus.org/CVCL_0320). U-2 OS cells contain high levels of chromosomal alteration and only few normal chromosomes are intact within the cell line's genome (American Type Culture Collection. U-2 OS. https://www.atcc.org/products/htb-96). PANC1 contains a deletion of *CDKN2A*, an Arg-273His mutation in *TP53*, and a mutation in *KRAS* (*SIB Swiss Institute of Bioinformatics. Cellosaurus PANC-1 (CVCL_0480). https://www.cellosaurus.org/CVCL_0480)*. All three lines are adherent.

CellTiter-Glo experiments

The cell viability experiments used to characterize trends in *in vitro* chemoresistance across a variety of seeding densities were performed using the CellTiter-Glo assay, which is an assay that assesses cell viability by indicating the amount of ATP present in a cell culture well. For these experiments, cancer cells were plated at the desired seeding densities in tissue-culture-treated black 96-well plates. 24 hours later, 20 µL of the desired chemotherapeutic agents were added at 6× the desired concentrations in order to generate solutions of the desired amount of drug in each well (because cells were generally plated in such a manner as to have 100 µL of cell solution in each well, the final volume of cell/drug solution in each well of the 96-well plate would be 120 µL - hence the dilution factor). Following 72 hours of treatment, 25 µL of the CellTiter-Glo reagent was added to each well of the cell culture plates and the results were collected using the Xenogen Ivis imaging system.

Ethidium homodimer staining

Cells were plated at the desired densities in a 48-well plate. 24 hours later, two 4 mL RPMI media solutions were prepared, into both of which was added 4 µL of ethidium homodimer at a 1 µM working concentration. Moreover, 12 µL of 3.33 mM cisplatin (for a final concentration of ~10 µM) was added into one of the solutions. This treated media, along with its untreated counterpart, was added to the appropriate wells on the plate. Following another 24 hours of treatment, results were imaged using fluorescence microscopy over the course of three days. Image analysis was conducted using the Fiji version of the ImageJ software.

Western blot analysis

TOV-21G cells were plated in a 12-well plate at the desired densities (the low-density cells were seeded at 150,000 cells/well, whereas the high-density cells were seeded at 600,000 cells/well). Following 48 hours of incubation, cells were harvested, lysed with RIPA, and quantified using the BCA assay. Subsequently, SDS-PAGE was performed to separate the proteins, which were then transferred onto a PVDF membrane. The appropriate primary and secondary antibodies were then used to probe for the indicated proteins, and the resulting membrane images were collected using a Syngene PXi instrument.

For western blot analysis of proteins in the apoptotic pathways, TOV-21G cells and OVMANA cells were separately plated in 12-well plates. Low-density cells were seeded at 50,000 cells/well and high-density cells were seeded at 600,000 cells/well. After 24 hours, cells in half of the trials were treated with cisplatin (2.5 µM for TOV-21G cells and 5.0 µM for OVMANA cells). The other half of trials were left untreated. At the subsequent 24, 48, and 72-hour timepoints, TOV-21G cells were harvested and three sets of five low-density replicates were pooled together to produce adequately concentrated samples for each timepoint. High-density samples were not pooled together. The slower growing OVMANA cells were harvested in the same manner following 72 hours of incubation. Lysis, quantification, SDS-PAGE gel electrophoresis, PVDF membrane transfer, and membrane imaging were performed as stated above.

Drug combination analysis

CellTiter-Glo analyses of drug combination effects on cell viability at varying densities were performed in a similar manner to how single drug effects were assessed (as described above), except that of course in these experiments the efficacy of both drugs was simultaneously analyzed. Cells were seeded at the

desired cell densities in tissue-culture-treated black 96-well plates. 24 hours later, 20 μL of the desired drugs were added at 7× the desired concentrations (the slight adjustment here is to account for the fact that there will be 140 μL of solution in each well rather than 120 μL of solution following treatment). As with the single-drug experiments, cells were treated for 72 hours, after which 25 μL of the CellTiter-Glo reagent was added to each well of the sample plates and results were collected using the Xenogen IVIS imaging system.

Regarding the interpretation of results from the combination experiments, the efficacy of drug combinations was generally assessed via plating a pair of drugs such that they form a dose-response matrix: in such a manner, the drug combination effects and how they vary with drug dose was determined. The degree of synergy, which is, in other words, a pair of drugs' ability to "work together" to produce an observed response, was found by comparing the observed combination response to the expected combination response as per the specifications of a given reference model for synergy calculation [1]. Indeed, a drug combination was generally assessed as either synergistic or antagonistic depending on how the observed response differs from this expected combination response [6].

Reference models used in evaluating a given drug combination included the Highest Single Agent (HSA) model, the Loewe additivity model, the Bliss independence model, and the Zero Interaction Potency (ZIP) model. Each of these reference models are characterized by different assumptions regarding the nature of the aforementioned expected combination response [1].

The HSA model, which is also known as Gaddum's non-interaction model, assumes that the expected combination response is equivalent to that of the drug with the higher individual effect at the dose in question. In this model, synergy would be the drug combination's ability to surpass this higher response. The Loewe additivity model defines the expected combination response as that which would be produced if a given drug in the analyzed combination were instead to be combined with itself. The Bliss independence model postulates the expected combination response as the result of a probabilistic interpretation of the individual drug responses in the combination as independent and competing events. Lastly, the ZIP synergy model builds a picture of the expected combination response by assuming that the two drugs in the combination should not produce a different dose-response curve than if each drug's dose-response patterns were assessed separately. In other words, under this model's assumptions regarding the expected combination response, the mathematical effect of adding a second drug to the dose-response curve of a first would be a mere shift in the baseline of the curve, and no significant change to its shape [6]. As is evident, each of these four models of drug combination efficacy are based on significantly different assumptions regarding the expected combination response, and the models' conception of this expected combination response influences how the synergy/antagonism score is calculated.

SynergyFinder (www.synergyfinder.org) is a web-based tool for evaluating the pre-clinical efficacy of pairwise drug combinations. Importantly, SynergyFinder incorporates each of the four synergy models discussed above in its analysis of drug combination efficacy and presents visually interpretable drug combination landscapes for the assessment of how two drugs interact in a given pre-clinical setting (*in vitro* cell culture for the purposes of this discussion) [1]. The drug combination experiments described herein have used SynergyFinder for the purposes of calculating the synergy score landscapes between the desired pair of drugs at varying seeding densities.

Results

Density-dependent chemoresistance is a trend observed across multiple combinations of cancer cell-lines and chemotherapeutic agents

Following preliminary cell culture assay results indicating that a cancer cell population's response to chemotherapy was seeding-density-dependent, the CellTiter-Glo assay was used to characterize the trend of cell viability/IC50 changes in response to cell seeding density variations with multiple cell lines and chemotherapeutic agents. Specifically, the responses of TOV-21G and OVMANA ovarian cancer cells to cisplatin, SW-480 cells to oxaliplatin, U-2 OS

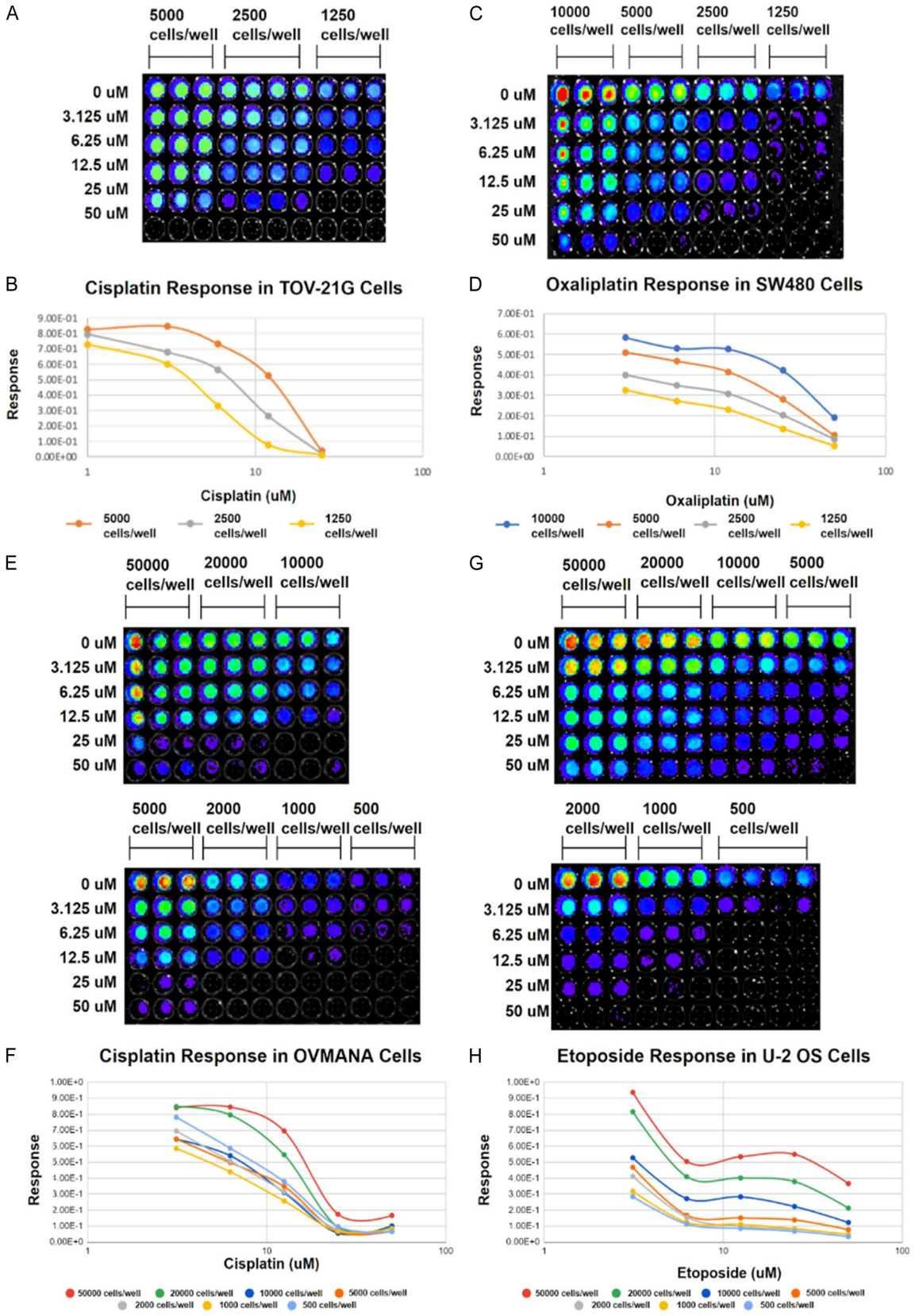
A
5000 cells/well
2500 cells/well
1250 cells/well
0 uM
3.125 uM
6.25 uM
12.5 uM
25 uM
50 uM
C
10000 cells/well
5000 cells/well
2500 cells/well
1250 cells/well
0 uM
3.125 uM
6.25 uM
12.5 uM
25 uM
50 uM
B
Cisplatin Response in TOV-21G Cells
Response
Cisplatin (uM)
5000 cells/well
2500 cells/well
1250 cells/well
D
Oxaliplatin Response in SW480 Cells
Response
Oxaliplatin (uM)
10000 cells/well
5000 cells/well
2500 cells/well
1250 cells/well
E
50000 cells/well
20000 cells/well
10000 cells/well
5000 cells/well
2000 cells/well
1000 cells/well
500 cells/well
0 uM
3.125 uM
6.25 uM
12.5 uM
25 uM
50 uM
G
50000 cells/well
20000 cells/well
10000 cells/well
5000 cells/well
2000 cells/well
1000 cells/well
500 cells/well
0 uM
3.125 uM
6.25 uM
12.5 uM
25 uM
50 uM
F
Cisplatin Response in OVMANA Cells
Response
Cisplatin (uM)
50000 cells/well
20000 cells/well
10000 cells/well
5000 cells/well
2000 cells/well
1000 cells/well
500 cells/well
H
Etoposide Response in U-2 OS Cells
Response
Etoposide (uM)
50000 cells/well
20000 cells/well
10000 cells/well
5000 cells/well
2000 cells/well
1000 cells/well
500 cells/well

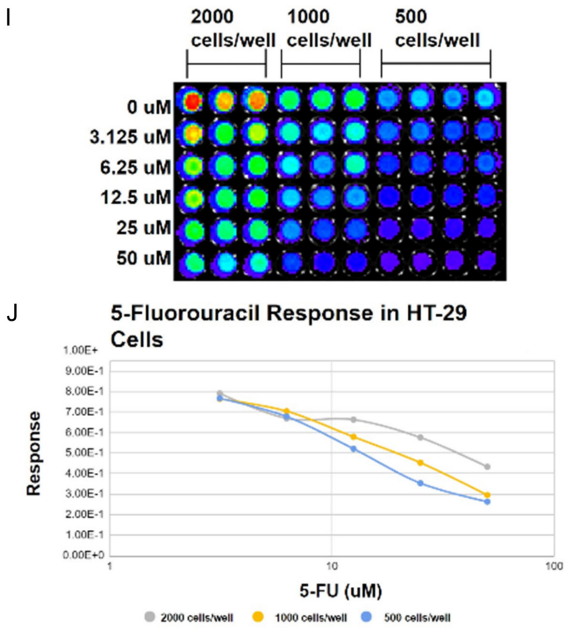

Figure 1. (A) CellTiter-Glo cell viability assay of TOV-21G cells plated at the indicated densities, treated with the indicated concentrations of cisplatin. (B) Dose-Response curve encapsulating the results shown in (A). (C) CellTiter-Glo viability assay of SW-480 cells plated at the indicated densities, treated with the indicated concentrations of oxaliplatin. (D) Dose-Response curve encapsulating the results shown in (C). (E) CellTiter-Glo viability assay of OV-MANA cells plated at the indicated densities, treated with the indicated concentrations of cisplatin. (F) Dose-Response curve encapsulating the results shown in (E). (G) CellTiter-Glo viability assay of U-2 OS cells plated at the indicated densities, treated with the indicated concentrations of etoposide. (H) Dose-Response curve encapsulating the results shown in (G). (I) CellTiter-Glo viability assay of HT-29 cells plated at the indicated densities, treated with the indicated concentrations of 5-FU. (J) Dose-Response curve encapsulating the results shown in (I).

cells to etoposide, and HT-29 cells to 5-FU were analyzed. IC50 calculations were performed using AAT Bioquest's IC50 Calculator. In nearly every cell/drug combination studied, very clear trends of increasing cell viability with increasing cell densities were found (**Figure 1**).

The IC50-Seeding Density Slope (ISDS) is a measurement of cancer cell chemosensitivity that incorporates density-dependent chemoresistance

Further exploration into how cellular response to chemotherapy is impacted by cell density changes led to an examination of how the chemotherapeutic IC50 varies with cancer cell seeding density. As referenced previously, He *et al*. found significant density-dependent variations in the IC50 of cisplatin in ovarian cancer cells [2]. Along those lines, based on the results of the experiments represented in **Figure 1**, the IC50 values of cisplatin and oxaliplatin were determined at the different seeding densities in TOV-21G ovarian cancer cells and SW480 colorectal cancer cells, respectively, in order to uncover any trends that might be observable in the aforementioned density-dependent IC50 variations. Remarkably, both cisplatin and oxaliplatin displayed a linear trend of increasing IC50 with increasing cancer cell densities (**Figure 2**).

While it remains to be seen whether this linear trend will hold with more replicates and in more drug/cell line combinations, these findings provide an initial glimpse into a novel means of assessing chemosensitivity in cancer cells: the IC50-Seeding Density Slope, or ISDS. This value was generated by determining the slope of the trendline in each of the seeding density/IC50 curves shown above (**Figure 2A** and **2B**). Because the ISDS comes from determining the IC50 of a given chemotherapeutic agent at multiple cell densities, it can assess chemosensitivity while taking density-dependent chemoresistance into account.

Cancer cells seeded at lower densities are more susceptible to chemotherapy-induced cell death

While the CellTiter-Glo assay is extremely useful for characterizing trends in cell viability under different conditions, its major limitation is that it cannot indicate the extent of cell death whatsoever. As a result, a weaker signal in a CellTiter-Glo assay cannot confidently be attributed to a greater extent of cell death, as it could also be due to a lower seeding density (i.e. there could be fewer viable cells following drug treatment because there were fewer cells seeded to begin with). To characterize the rate of cell death in sparsely-seeded cell populations as compared to that in densely-seeded

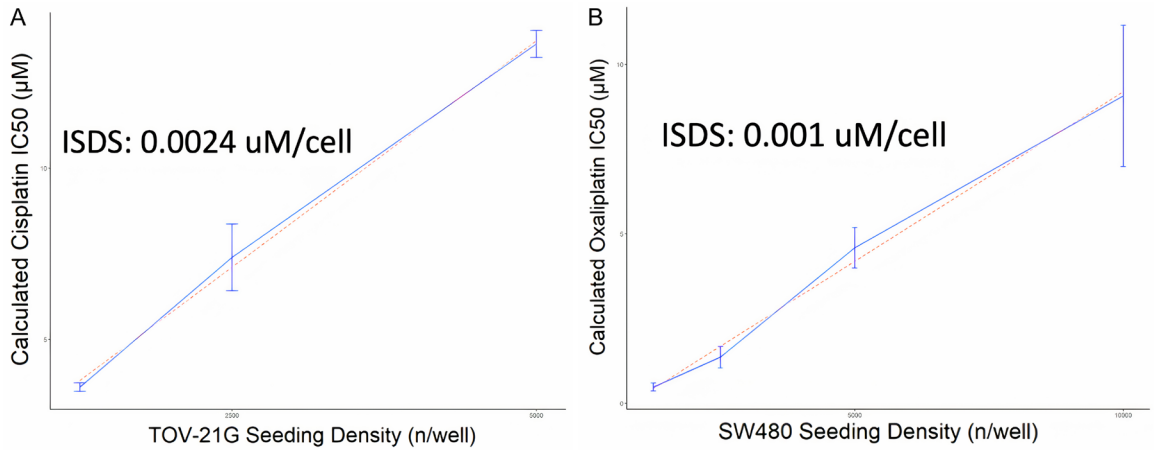

Figure 2. A. IC50-Seeding Density relationship for TOV-21G cells treated with cisplatin. B. IC50-Seeding Density relationship for SW-480 cells treated with oxaliplatin with an overlaid least-squares linear regression (red dashed line). Error bars represent ±1 SEM. The slope of this trendline (the ISDS) is indicated for each graph. Graphs were generated with the help of Andrew George.

cell populations, an ethidium homodimer staining experiment was performed, wherein TOV-21G and OVMANA cells were separately plated at varying densities, treated with cisplatin, and subsequently stained with ethidium homodimer (which identifies dead cells). The cells were then imaged over the course of three days following cisplatin treatment. As expected based on the previously conducted cell viability experiments, compared to the more densely-seeded cancer cells, a greater amount of ethidium homodimer staining was observed in the sparsely-seeded wells (**Figure 3A-D**), implying that the sparsely-seeded cells are less resistant to chemotherapy-induced cell death.

Levels of autophagic activity are modulated by changes in cancer cell seeding density

At the same time, possible intracellular mechanisms of density-dependent chemoresistance were explored. A western blot analysis was conducted wherein cells were plated at high and low densities and several markers of cell survival pathways were assessed.

Notably, levels of p62, a multifunctional protein commonly used as a reporter of autophagy activity [7], were decreased in every replicate of the higher cell densities tested (**Figure 4A**). Additionally, considering the underloading evident in the sixth lane (marked by the red arrow), there is also a noticeable upregulation of the anti-apoptotic protein BCL2 in the high-density cells (**Figure 4A**). Given that BCL2 is correlated with cell survival, an increase in the levels of BCL2 would indicate that high density cells have less flux through the autophagy pathway, thus providing an additional explanation for their increased survival in response to chemotherapy [8].

Within the context of autophagy, p62, also known as sequestosome 1 (SQSTM1), is a classical receptor, known to be recruited to polyubiquitinated protein aggregates and form complexes that are degraded by the autophagy machinery [9]. Importantly, this means that p62 levels are inversely correlated with levels of autophagy, and thus lower p62 levels at higher seeding densities would indicate greater autophagic flux at higher cell densities (**Figure 4A**). In order to verify this hypothesis and further investigate the implications of the observed p62 modulation by cell density, experiments to analyze how autophagy is impacted by cell density and to determine if autophagy plays a role in density-dependent chemoresistance were conducted. Accordingly, the effect of the autophagy inhibitor chloroquine on TOV-21G, SW480, and U-2 OS cell viabilities at varying seeding densities was assessed in a CellTiter-Glo assay (**Figure 4B-J**).

As is shown, chloroquine was found to induce a greater reduction in cancer cell viability at the lower cell density as compared to the higher cell density. Chloroquine's decreased effectiveness at reducing cell viability in the higher cell density population would correspond to an

A

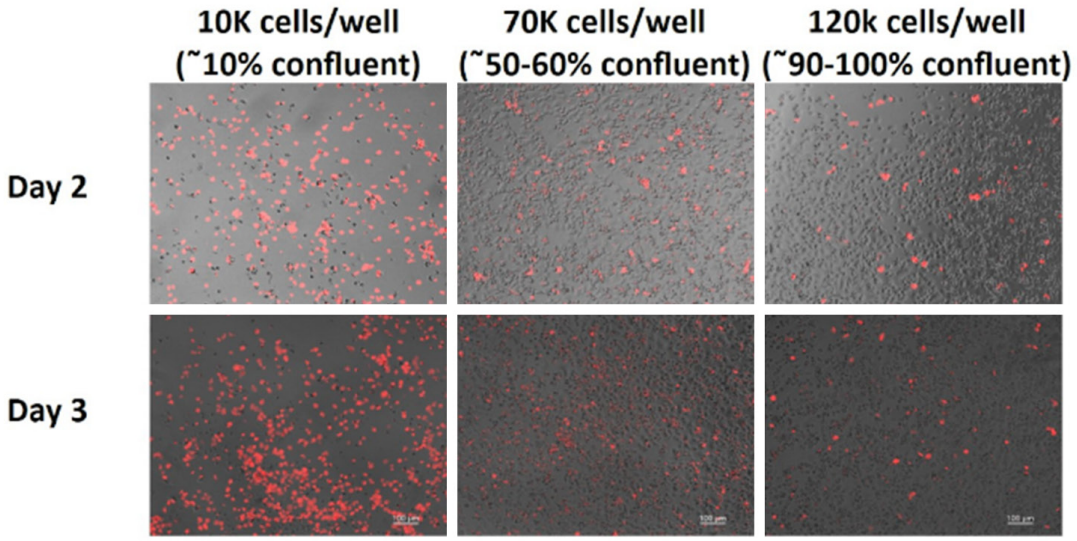
10K cells/well
(~10% confluent)
70K cells/well
(~50-60% confluent)
120k cells/well
(~90-100% confluent)
Day 2
Day 3

B

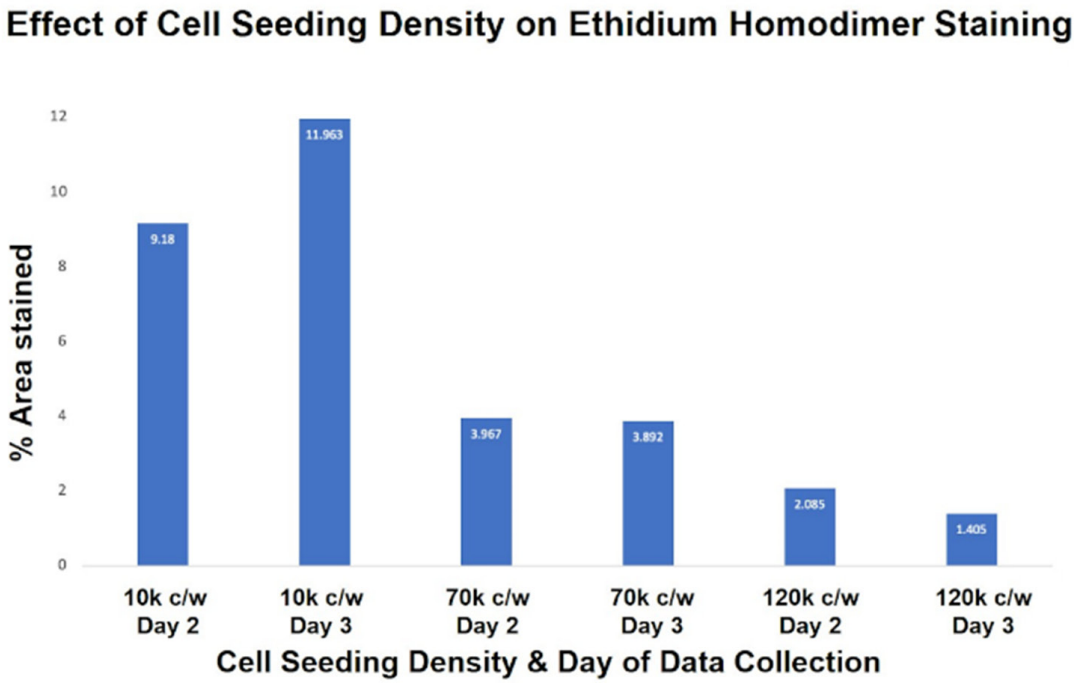
Effect of Cell Seeding Density on Ethidium Homodimer Staining
% Area stained
0
2
4
6
8
10
12
9.18
11.963
3.967
3.892
2.085
1.405
10k c/w Day 2
10k c/w Day 3
70k c/w Day 2
70k c/w Day 3
120k c/w Day 2
120k c/w Day 3
Cell Seeding Density & Day of Data Collection

C

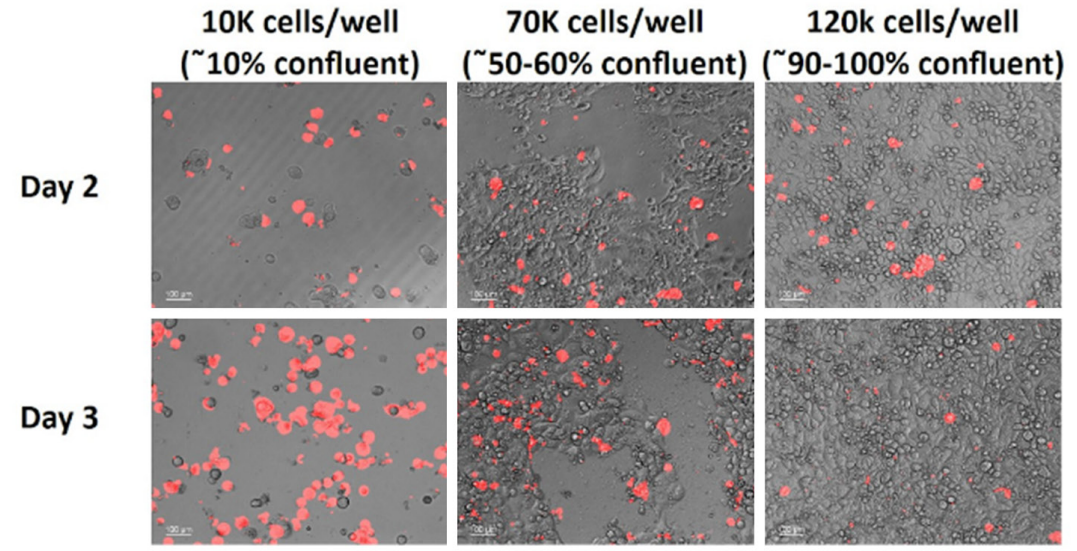
10K cells/well
(~10% confluent)
70K cells/well
(~50-60% confluent)
120k cells/well
(~90-100% confluent)
Day 2
Day 3

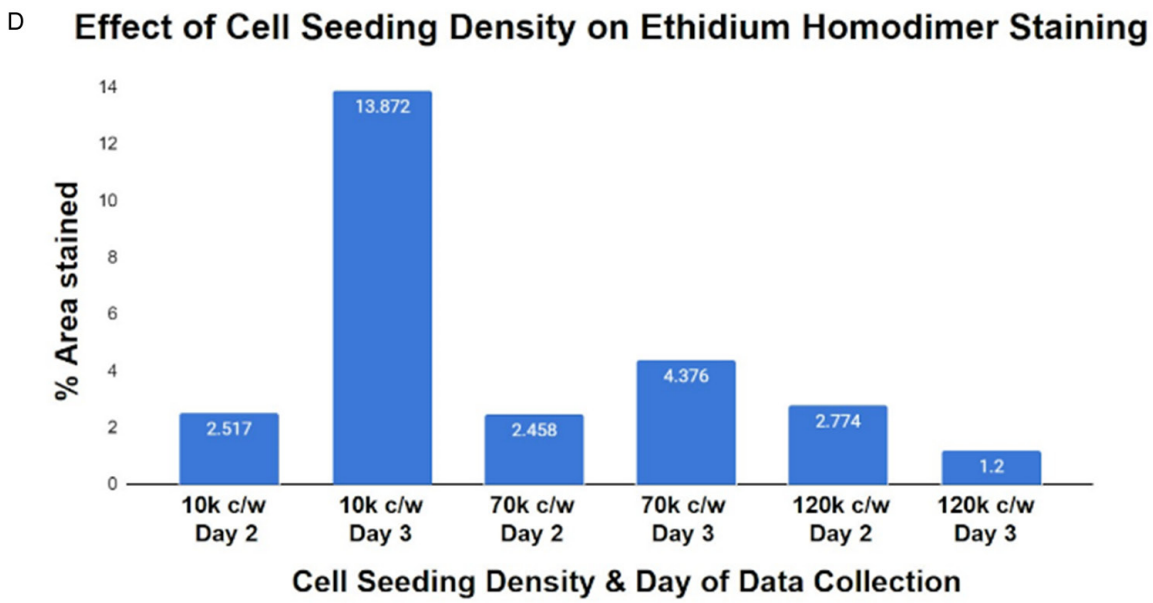

Figure 3. (A) Fluorescence microscopy images of ethidium homodimer-stained TOV-21G cells at varying densities that have been treated with cisplatin for either two or three days. Scale bar is equal to 100 micrometers. (B) Quantification of ethidium homodimer staining in each well shown in (A) as a percent of the total well area. Wells are sorted first by their cell density and the day they were analyzed (either day 2 or day 3). (C) Fluorescence microscopy images of ethidium homodimer-stained OVMANA cells at varying densities that have been treated with cisplatin for either two or three days. Scale bar is equal to 100 micrometers. (D) Quantification of ethidium homodimer staining in each well shown in (C) as a percent of the total well area. Wells are sorted first by their cell density and the day they were analyzed (either day 2 or day 3).

increased autophagic flux in these higher cell density cells because, if there is a greater autophagic flux in these cells, more chloroquine would be required to sufficiently inhibit autophagic activity and thus eliminate the cancer cell, and that is what is observed (**Figure 4D**, **4I** and **4J**). As a result, the findings from the chloroquine cell viability assay presented here correspond with the results from the western blot results discussed earlier (**Figure 4A**), in that autophagic flux may increase with cell density.

Increased autophagy may be a key component of density-dependent chemoresistance in some cancer cells

Having shown that autophagy may be regulated by changes in cell density (in that autophagic flux increases at higher cell densities), the logical next step became how this increased autophagy could play a role in the phenomenon of density-dependent chemoresistance. To that end, a CellTiter-Glo experiment was performed wherein TOV-21G cells at high and low densities were treated with a combination of chloroquine and cisplatin, in order to investigate how autophagy inhibition can affect density-dependent chemoresistance (**Figure 6A-D**, **6M** and **6N**).

At both the higher and lower cell densities, chloroquine and cisplatin exhibited a significant amount of synergy in reducing TOV-21G cancer cell viability (**Figure 6B** and **6D**). In addition, in three out of four synergy calculation methodologies, the magnitude of synergistic cell viability reduction was found to be greater for the lower density cells than for the higher density cells, implying that sparsely-seeded cells are more sensitive to autophagy inhibition as a means of increasing chemosensitivity (**Figure 6M** and **6N**). As a side note, **Figure 6M** and **6N** were split to accommodate for the vastly different scale of the Loewe and HSA synergy scores as compared to the ZIP and Bliss synergy scores.

Similar experiments were also performed using chloroquine and oxaliplatin combinations in SW480 cells as well as chloroquine and etoposide in U-2 OS cells (**Figure 6E-L**, **6O** and **6P**).

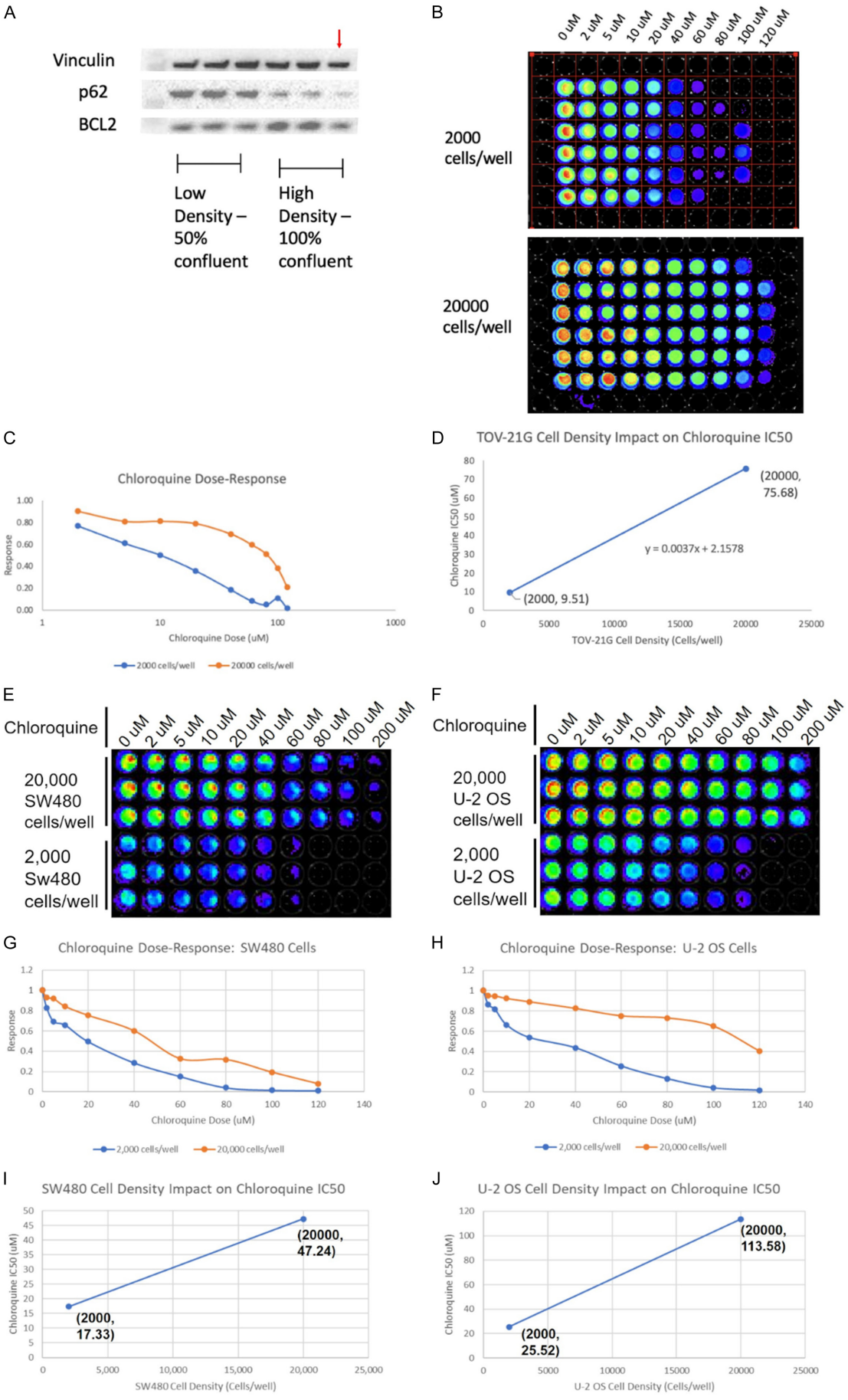
A
Vinculin
p62
BCL2
Low Density – 50% confluent
High Density – 100% confluent
B
0 uM
2 uM
5 uM
10 uM
20 uM
40 uM
60 uM
80 uM
100 uM
120 uM
2000 cells/well
20000 cells/well
C
Chloroquine Dose-Response
Response
Chloroquine Dose (uM)
2000 cells/well
20000 cells/well
D
TOV-21G Cell Density Impact on Chloroquine IC50
Chloroquine IC50 (uM)
(20000, 75.68)
y = 0.0037x + 2.1578
(2000, 9.51)
TOV-21G Cell Density (Cells/well)
E
Chloroquine
20,000 SW480 cells/well
2,000 Sw480 cells/well
F
Chloroquine
20,000 U-2 OS cells/well
2,000 U-2 OS cells/well
G
Chloroquine Dose-Response: SW480 Cells
Response
Chloroquine Dose (uM)
2,000 cells/well
20,000 cells/well
H
Chloroquine Dose-Response: U-2 OS Cells
Response
Chloroquine Dose (uM)
2,000 cells/well
20,000 cells/well
I
SW480 Cell Density Impact on Chloroquine IC50
Chloroquine IC50 (uM)
(20000, 47.24)
(2000, 17.33)
SW480 Cell Density (Cells/well)
J
U-2 OS Cell Density Impact on Chloroquine IC50
Chloroquine IC50 (uM)
(20000, 113.58)
(2000, 25.52)
U-2 OS Cell Density (Cells/well)

Figure 4. (A) Levels of p62 and BCL2 at different TOV-21G cell densities. Data from three replicates, each seeded and harvested separately, were collected for each experimental condition; these are indicated in the blot. The arrow marks the sixth lane of the blot, which was underloaded. This was taken into consideration when assessing the protein expression trends presented in the blot. (B) CellTiter-Glo assay of low-density (2,000 cells/well; top) and high-density (20,000 cells/well; bottom) TOV-21G cell viability in response to increasing concentrations of chloroquine treatment. (C) Dose-response curve summarizing the results from (B) and illustrating how chloroquine impacts TOV-21G cell viability (as indicated by CellTiter-Glo response on the y-axis) at different cell densities. (D) IC50-cell density curve summarizing the results from (B) and illustrating how the chloroquine IC50 in TOV-21G cells increases with cell seeding density. More specifically, the IC50 of chloroquine in the 2,000 cells/well population was found to be 9.51 μM, whereas the IC50 of chloroquine in the 20,000 cells/well population was found to be 75.68 μM. (E) CellTiter-Glo assay of low-density (2,000 cells/well) and high-density (20,000 cells/well) SW480 cell viability in response to increasing concentrations of chloroquine treatment. (F) CellTiter-Glo assay of low-density (2,000 cells/well) and high-density (20,000 cells/well) U-2 OS cell viability in response to increasing concentrations of chloroquine treatment. (G) Dose-response curve summarizing the results from (E) and illustrating how chloroquine impacts SW480 cell viability (as indicated by CellTiter-Glo response on the y-axis) at different cell densities. (H) Dose-response curve summarizing the results from (F) and illustrating how chloroquine impacts U-2 OS cell viability (as indicated by CellTiter-Glo response on the y-axis) at different cell densities. (I) IC50-cell density curve summarizing the results from (E) and illustrating how the chloroquine IC50 in SW480 cells increases with cell seeding density. More specifically, the IC50 of chloroquine in the 2,000 cells/well population was found to be 17.33 μM, whereas the IC50 of chloroquine in the 20,000 cells/well population was found to be 47.24 μM. (J) IC50-cell density curve summarizing the results from (F) and illustrating how the chloroquine IC50 in U-2 OS cells increases with cell seeding density. More specifically, the IC50 of chloroquine in the 2,000 cells/well population was found to be 25.52 μM, whereas the IC50 of chloroquine in the 20,000 cells/well population was found to be 113.58 μM.

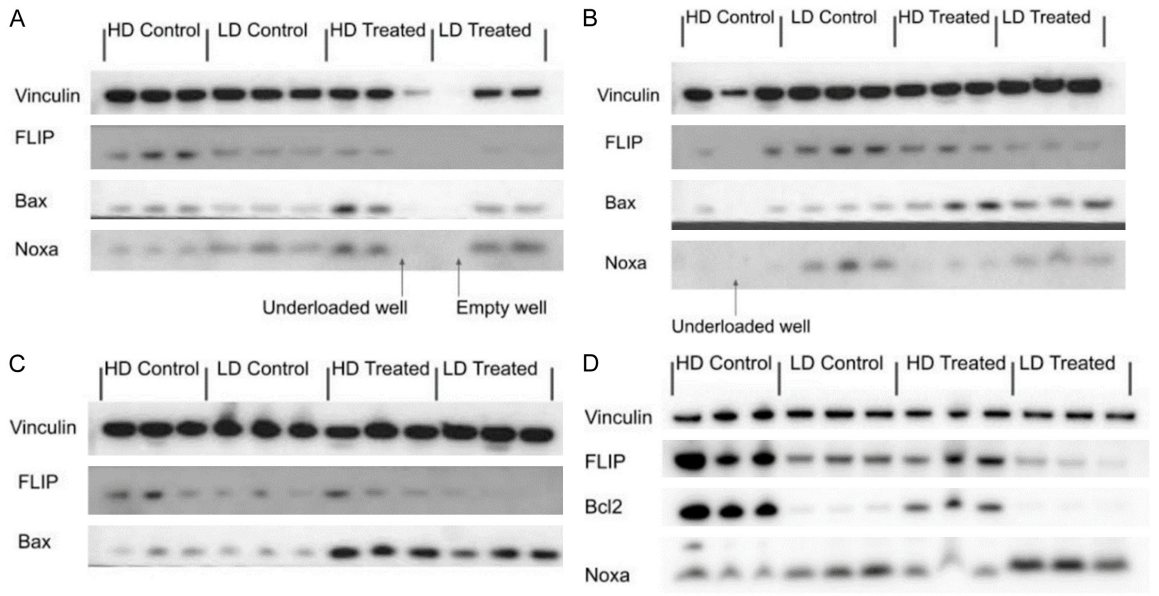

Figure 5. A. Levels of c-FLIPL, Bax, and Noxa at different TOV-21G cell densities and treatment groups at 24 hours. "HD" stands for high density seeding conditions (100% confluent). "LD" stands for low density seeding conditions (~40% confluent at 24 hours). Data from three replicates, each seeded and harvested separately, were collected for each experimental condition; these are indicated in the blot. Additionally, for each low-density replicate, five low density sample harvests needed to be pooled together to obtain a lysate that was concentrated enough for western blotting. The arrows mark the ninth lane and tenth lanes of the blot, which were underloaded and empty respectively. This was taken into consideration when assessing the protein expression trends presented in the blot. B. Levels of c-FLIPL, Bax, and Noxa at different TOV-21G cell densities and treatment groups at 48 hours. "HD" stands for high density seeding conditions (100% confluent). "LD" stands for low density seeding conditions (~70-80% confluent at 48 hours). Data from three replicates, each seeded and harvested separately, were collected for each experimental condition; these are indicated in the blot. Additionally, for each low-density replicate, five low density sample harvests needed to be pooled together to obtain concentrated lysates. The arrow marks the second lane of the blot, which was underloaded. This was taken into consideration when assessing the protein expression trends presented in the blot. C. Levels of c-FLIPL and Bax at different TOV-21G cell densities and treatment groups at 72 hours. "HD" stands for high density seeding conditions (100% confluent). "LD" stands for low density seeding conditions (~90-100% confluent at 72 hours). Data from three replicates, each seeded and harvested separately, were collected

for each experimental condition; these are indicated in the blot. Additionally, for each low-density replicate, five low density sample harvests were pooled together to be consistent with the 24 and 48hours low density harvest protocol. D. Levels of c-FLIPL, Bcl2, and Noxa at different OVMANA cell densities and treatment groups at 72 hours. "HD" stands for high density seeding conditions (100% confluent). "LD" stands for low density seeding conditions (~50% confluent at 72 hours). Data from three replicates, each seeded and harvested separately, were collected for each experimental condition; these are indicated in the blot. Additionally, for each low-density replicate, five low density sample harvests needed to be pooled together to obtain a lysate that was concentrated enough for western blotting.

Although both combinations did work together to reduce cell viability, neither combination displayed mean synergy overall. All mean synergy scores for both combinations averaged between -10 and +10, suggesting additive drug interaction (**Figure 6F**, **6H**, **6J**, **6L**, **6O** and **6P**). It must be noted that there were some local pockets of synergy, where some concentration combinations of oxaliplatin and chloroquine or etoposide and chloroquine produced local synergy scores greater than 10, indicated by a deeper color of red in **Figure 6F**, **6H-J**. Despite these local synergistic effects, overall synergistic drug interactions were not strong enough or consistent enough to raise the mean synergy score above 10. Therefore, regardless of cell density, autophagy inhibition by chloroquine was unable to sufficiently sensitize SW480 cells or U-2 OS cells to oxaliplatin or etoposide, respectively.

Changes in tumor cell seeding density affects apoptotic protein expression

Expression of BCL2 was also probed in OVMANA ovarian carcinoma cells. At 72 hours, levels of BCL2 were substantially increased in both untreated and cisplatin-treated high density OVMANA cells when compared to the respective low density OVMANA groups. This finding supported the previous data from TOV-21G cells that BCL2 is upregulated in high density cells relative to low density cells.

Given the evidence that BCL2 was upregulated with increased seeding conditions, western blot analyses of other apoptosis-related proteins were performed. Noxa and BCL2-associated X protein (Bax) are pro-apoptotic proteins in the BCL2 family, which act in the intrinsic apoptotic pathway [10, 11]. Both Noxa and Bax displayed modulations in expression according to cell density, treatment, and time. Noxa appeared to be overexpressed in untreated, low density TOV-21G cells at both 24 and 48 hour time points compared to untreated, high density TOV-21G cells (**Figure 6A** and **6B**). At 48 hours, Noxa expression is also increased in low density TOV-21G cells treated with cisplatin relative to high density TOV-21G cells treated with the drug at the same time point (**Figure 5B**). The trend of Noxa being overexpressed in low density cells is also supported by western blot analysis of OVMANA cells at 72 hours, which show greater Noxa expression in treated, low density cells compared to treated, high density cells (**Figure 5D**). Bax appears elevated in both treated and untreated high density TOV-21G cells relative to their respective low-density groups at 24 hours (**Figure 5A**). After 48 hours, the level of Bax in all untreated TOV-21G cells becomes equivalent; similarly, Bax expression in treated TOV-21G cells at 72 hours also appears to converge, albeit at a higher level of expression compared to untreated cells (**Figure 5B** and **5C**). Cisplatin treatment is known to increase Bax expression by first inducing p53 expression, which in turn, induces the expression of Bax [12, 13]. Therefore, it would be expected that cells treated with cisplatin would display an increase in Bax compared to untreated cells.

Cellular FLICE (FADD-like IL-1β-converting enzyme)-inhibitory protein (c-FLIP) is an antiapoptotic protein in the extrinsic apoptosis pathway and is present in short, long, and spliced forms in cells [14]. 55 kDa long form c-FLIP (c-FLIPL) was found to be elevated in untreated, high density TOV-21G cells at 24 and 72 hours compared to the untreated, low density TOV-21G samples at the same time points (**Figure 5A** and **5C**). At 48 hours, c-FLIPL expression appeared to be slightly greater in untreated, low density TOV-21G cells compared to the untreated, high density TOV-21G counterparts (**Figure 5B**). c-FLIPL also appeared to be slightly increased in high density TOV-21G cells treated with cisplatin at 72 hours compared to treated, low density TOV-21G cells at the same time point (**Figure 5C**). The OVMANA cell line displayed similar results, as c-FLIPL was overexpressed in both high-density groups at 72 hours relative to low density OVMANA cells with

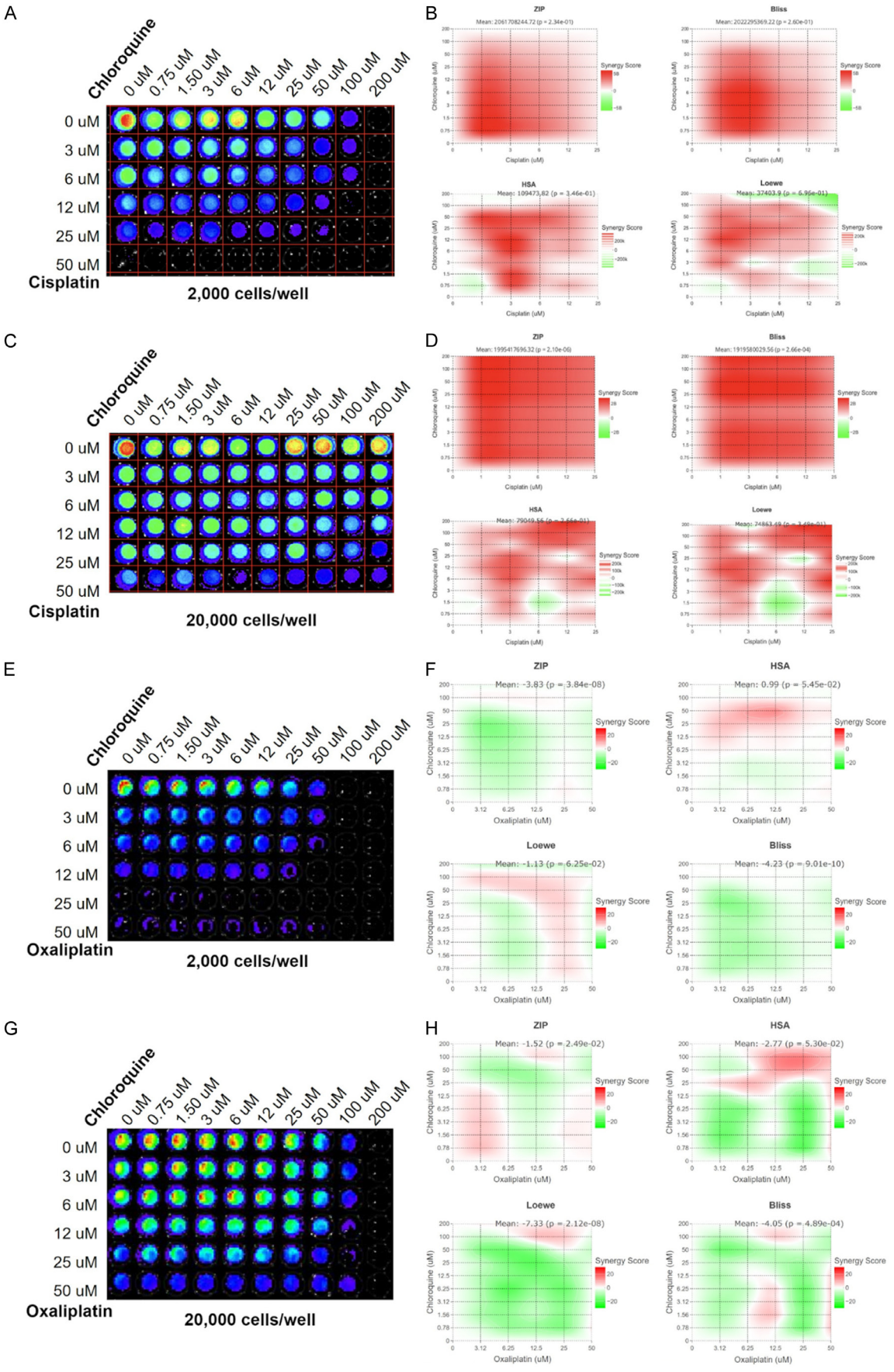
A
Chloroquine
0 uM
0.75 uM
1.50 uM
3 uM
6 uM
12 uM
25 uM
50 uM
100 uM
200 uM
0 uM
3 uM
6 uM
12 uM
25 uM
50 uM
Cisplatin
2,000 cells/well
B
ZIP
Bliss
HSA
Loewe
Synergy Score
Chloroquine (uM)
Cisplatin (uM)
C
20,000 cells/well
D
E
Oxaliplatin
2,000 cells/well
F
Oxaliplatin (uM)
G
20,000 cells/well
H

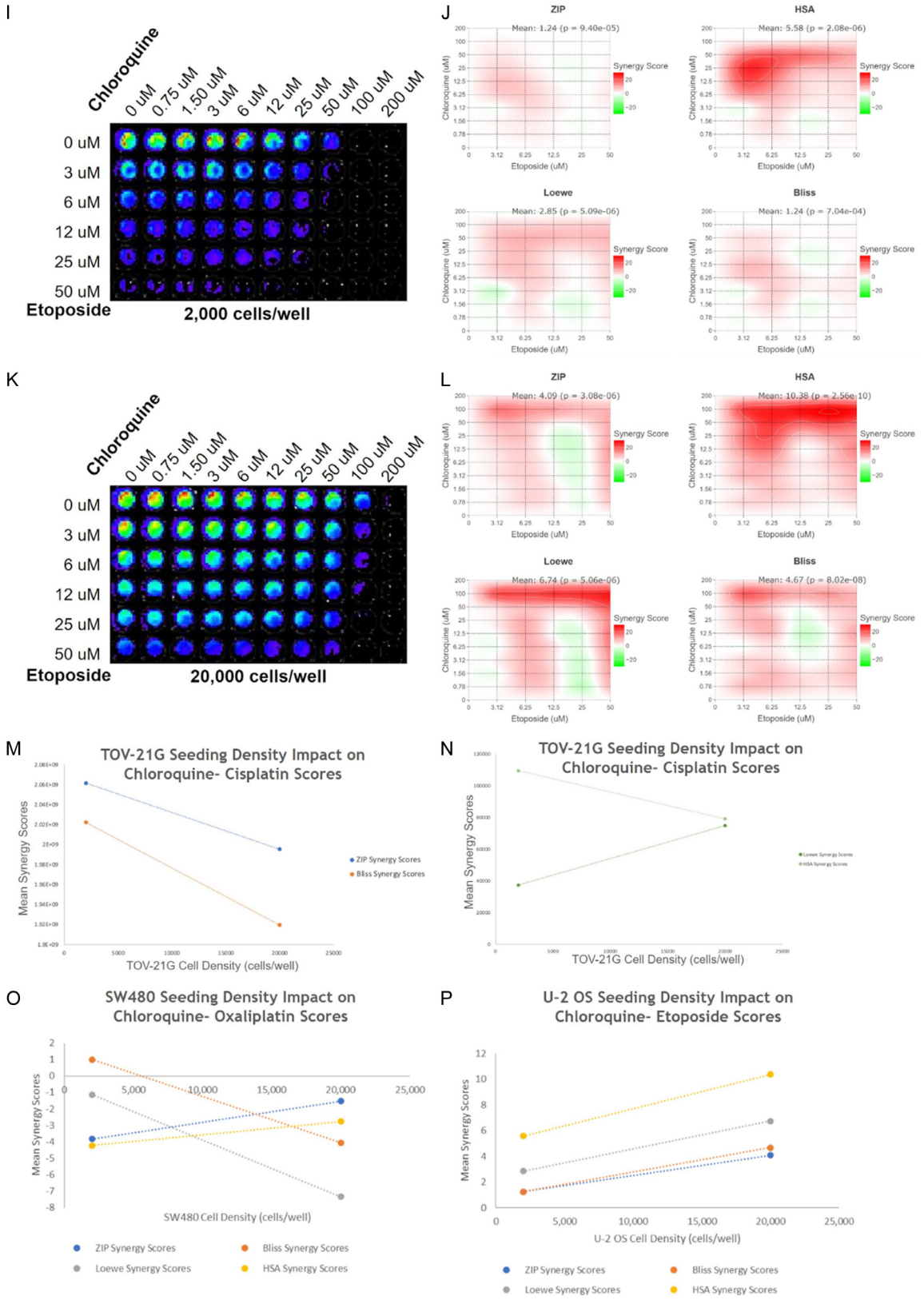

Figure 6. A. CellTiter-Glo assay of low-density TOV-21G cells treated with chloroquine and cisplatin at the indicated concentrations. B. Different methodologies of synergy analysis (ZIP, top right; Bliss, top left; HSA, bottom left; Loewe, bottom right) for the combination of chloroquine and cisplatin on low-density TOV-21G cells. C. CellTiter-Glo assay of high-density TOV-21G cells treated with chloroquine and cisplatin at the indicated concentrations. D. Four differ-

ent methodologies of synergy analysis (ZIP, top right; Bliss, top left; HSA, bottom left; Loewe, bottom right) for the combination of chloroquine and cisplatin on high-density (20,000 cells/well) TOV-21G cells. E. CellTiter-Glo assay of low-density SW480 cells treated with chloroquine and oxaliplatin at the indicated concentrations. F. Different methodologies of synergy analysis (ZIP, top right; HSA, top left; Loewe, bottom left; Bliss, bottom right) for the combination of chloroquine and oxaliplatin on low-density SW480 cells. G. CellTiter-Glo assay of high-density SW480 cells treated with chloroquine and oxaliplatin at the indicated concentrations. H. Four different methodologies of synergy analysis (ZIP, top right; HSA, top left; Loewe, bottom left; Bliss, bottom right) for the combination of chloroquine and oxaliplatin on high-density (20,000 cells/well) SW480 cells. I. CellTiter-Glo assay of low-density U-2 OS cells treated with chloroquine and etoposide at the indicated concentrations. J. Different methodologies of synergy analysis (ZIP, top right; HSA, top left; Loewe, bottom left; Bliss, bottom right) for the combination of chloroquine and etoposide on low-density U-2 OS cells. K. CellTiter-Glo assay of high-density U-2 OS cells treated with chloroquine and etoposide at the indicated concentrations. L. Four different methodologies of synergy analysis (ZIP, top right; HSA, top left; Loewe, bottom left; Bliss, bottom right) for the combination of chloroquine and etoposide on high-density (20,000 cells/well) U-2 OS cells. M. Curve depicting the impact of variations in TOV-21G cell density on two different synergy measurements (ZIP and Bliss, indicated on the graph) of a chloroquine-cisplatin combination treatment *in vitro*. N. Curve depicting the impact of variations in TOV-21G cell density on two different synergy measurements (Loewe and HSA, indicated on the graph) of a chloroquine-cisplatin combination treatment *in vitro*. O. Curve depicting the impact of variations in SW480 cell density on four different synergy measurements (ZIP, Bliss, HSA, and Loewe indicated on the graph) of a chloroquine-oxaliplatin combination treatment *in vitro*. P. Curve depicting the impact of variations in U-2 OS cell density on four different synergy measurements (ZIP, Bliss, HSA, and Loewe indicated on the graph) of a chloroquine-etoposide combination treatment *in vitro*.

respective treatments (**Figure 5D**). In the majority of these cases, c-FLIPL appears to be upregulated in cells seeded at higher densities compared to those seeded at lower densities.

Discussion

Our experimental results have important implications regarding the nature of density-dependent chemoresistance in cancer cells.

Regarding the initial CellTiter-Glo experiments described in **Figure 1**: Clearly, there is an effect of the seeding density on the determined IC50 for the indicated cell line/drug combinations. These results undoubtedly suggest that chemoresistance in different cancer cell lines is density-dependent. In addition, the results of the ethidium homodimer staining assay are further support for the importance of seeding density in determining a cell population's response to chemotherapy *in vitro*, as chemotherapy-induced cell death was shown to be directly influenced by the density at which a given cancer cell population was seeded.

An interesting finding from the western blot results presented in this study is that apoptotic proteins are regulated merely by cell density fluctuations. Both BCL2 and c-FLIPL appear to increase at the higher cell density levels, while NOXA seems to be elevated in cells of lower density (**Figures 4A** and **5**). BCL2 and NOXA are antiapoptotic and proapoptotic members, respectively, of the BCL2 protein family that is highly expressed in cancer cells [8, 10]. Furthermore, c-FLIPL is a known antiapoptotic protein in the extrinsic apoptotic pathway [14]. As a result, an increase in BCL2 and c-FLIPL with cell density could provide an explanation of the heightened survival of high-density cells in response to chemotherapy, in that apoptotic activity decreases. Similarly, the inverse relationship between NOXA expression and cell density could further illustrate why lower density tumor cells experience more chemotherapy-induced cell death; low density cells may have increased apoptotic activity through NOXA overexpression. If this is indeed the case, then further experiments would be necessary to ascertain exactly how apoptosis is regulated by cell density (i.e. to further elucidate connections between the integrin or cadherin pathways and the apoptosis pathway, etc.), and the implications that apoptosis modulation would bear for targeting density-dependent chemoresistance. It is also important to note that under certain circumstances, such as increased death receptor activation or elevated levels of short form and splice form c-FLIP, c-FLIPL can also act as a proapoptotic protein [14]. Therefore, characterization of death receptor expression and other c-FLIP isoforms under different seeding conditions will be necessary to better understand the role of c-FLIPL in density-dependent drug resistance.

Additionally, there is clearly some effect of cell density on autophagic activity, as evidenced by the apparent changes in p62 levels between

cell densities (**Figure 4A**). This connection between cell seeding density and autophagic activity has been hinted at in previous studies. In their work, He *et al*. examined the role of several different chemoresistance-related pathways in density-dependent chemoresistance, such as cell adherence (through analysis of levels of E-cadherin, N-cadherin, and β-catenin), autophagy (through analyzing levels of LC3b and p62), apoptosis (via quantifying Bax, Bcl-2, and p-Bad/Bad), and the PI3K signaling pathway (through analyzing levels of pAkt/Akt). From these analyses, He et al. were able to develop an IC50-fitting formula and an IHC scoring method which both used levels of pAkt and p62 as benchmarks [2].

In addition, Trajkovic *et al*. found that expression levels of the autophagic markers p62 and LC3II were altered in confluent cell populations: these molecular variations were attributed to nutrient depletion and cell crowding leading to changes in the mTOR signaling pathway [15]. While these studies did affirm the importance of p62 in density-dependent chemoresistance, they were not able to produce evidence supporting broader claims regarding the relationship of autophagic flux with density-dependent chemoresistance. On the other hand, not only do the results of this study verify that p62 levels are affected by cell seeding density, but they also suggest that autophagy levels are tied to cell density and that autophagy may play a role in density-dependent chemoresistance (in that inhibition of autophagy could increase the efficacy of chemotherapeutic drugs, especially at lower densities).

The findings from the CellTiter-Glo assay indicating that chloroquine is less effective at reducing cell viability at higher cell densities than at lower cell densities would be consistent with the notion from the p62 western blot that autophagic flux is increased at higher cell densities - in this context, a greater concentration of chloroquine would be necessary to reduce cell viability at higher cell densities because there is more autophagic flux at the higher cell densities; on the other hand, because there is less autophagic flux at the lower cell densities, a lower concentration of chloroquine would be required to completely inhibit the autophagic pathway and induce cell death. In this manner, results from the chloroquine CellTiter-Glo assay (**Figure 4B-J**) suggest that autophagic flux is density-dependent in TOV-21G, SW480, and U-2 OS cancer cells.

Moreover, this study's findings from the chloroquine-cisplatin combination experiment (**Figure 6A-D**, **6M**, **6N**) not only indicate that lower autophagic flux could explain the increased sensitivity of some low-density cancer cells to chemotherapy but also suggest that autophagy inhibition may be important for increasing the efficacy of some anti-cancer chemotherapeutic strategies.

Despite these findings and the implications they bear for the analysis of density-dependent chemoresistance in cancer cells, there are still shortcomings with the experimental approaches that adversely impacted the strength of the results. Perhaps most importantly, our results rely heavily on the CellTiter-Glo assay of cell viability, which is susceptible to inconsistency in observed data and which is often influenced by a phenomenon known as the "edge effect", wherein cells in wells along the edges of a tissue culture plate tend to behave differently from cells in wells toward the center. Although care was taken to mitigate this edge effect as much as possible, it would be difficult to say that it had no impact whatsoever on the results of the experiments described herein.

While both the experiments of He *et al.* and those of this study focused largely on the analysis of the chemosensitivity of cisplatin in ovarian cancer cells (He *et al*. used SKOV-2, ES-2, HO8910, A2780, and A2780DR, while we used TOV-21G and OVMANA, along with SW-480, HT-29, U-2 OS, and PANC1), He *et al.* argue that the results of any analysis into density-dependent chemoresistance will have broad implications for other chemotherapeutic agents and cancer systems, (1) because the intracellular signaling pathways studied for explaining density-dependent chemoresistance of cisplatin in ovarian cancer cells are also targeted by other chemotherapeutic agents in other cell lines, and, on a broader level, (2) because the phenomenon of density-dependent chemoresistance has been observed in several different cancer cell lines treated with several different chemotherapeutic agents[2]. Nevertheless, repeating the experiments described herein with a variety of different cancer cell lines and chemotherapeutic drugs will further establish the

relevance of these findings to the phenomenon of density-dependent chemoresistance in general.

Additionally, the methods to analyze autophagy and its impact on density-dependent chemoresistance in our study are somewhat limited, in that the only means by which autophagic flux has been assessed is through p62 levels and chloroquine sensitivity. While these are undoubtedly common means of studying autophagy, further experiments with alternative techniques, such as monodansylcadaverine staining, which assesses autophagy activation by labeling acidic endosomes, lysosomes, and autophagosomes [16], and trehalose-mediated autophagy induction [17], which can be used in combination with cisplatin treatment to ascertain the protective effects of autophagic flux in cancer cells, will strengthen this study's conclusions regarding autophagy's connections to density-dependent chemoresistance.

Further studies will focus on going deeper into the connection between autophagic flux and density-dependent chemoresistance. More specifically, while the experiments described in this study suggest that autophagic flux is modulated by cancer cell seeding density and imply that it may be the causative process behind density-dependent chemoresistance, exactly how and why autophagic activity increases with higher cell densities, and how this increased autophagic flux could cause heightened chemotherapy resistance, remain yet to be explored. Potential experiments to address these topics might involve western blots and other molecular analyses exploring how pathways involved in cell-cell contact are affected by autophagy inhibition, in order to uncover connections between cell density and autophagic flux. In addition, shotgun proteomic analyses of cancer cells at varying densities upon chemotherapeutic treatment and upon autophagy inhibition could be useful for investigating not only how the molecular effects of a given chemotherapeutic drug are regulated by cell density but also how autophagic flux at these different densities might impact a drug's ability to bring about its intended effect on the cell. Moreover, ongoing studies are focused on examining the relationship between seeding density and anticancer chemotherapeutic synergy. This study's findings from the chloroquine/cisplatin combination experiments suggest that the synergistic efficacy of a combination of chemotherapeutic agents should decrease at higher cell densities, but the actual effect of cell density on chemotherapeutic synergy, if there is one, remains to be seen. These experiments would provide a novel angle to the field of density-dependent chemoresistance research.

Alternative mechanisms of density-dependent chemoresistance

Of course, increased autophagic flux is not the only possible mechanism underlying density-dependent chemoresistance in cancer cells. Perhaps the most important mechanism involved could be a regulation of apoptosis by cell density variations, as suggested by the modulation of BCL2, c-FLIPL, and NOXA levels presented in **Figures 4A** and **5**. To this end, future mechanistic studies of density-dependent chemoresistance would involve understanding how apoptosis could be targeted to attenuate therapy resistance at varying cell densities. Additionally, pathways of cell-cell contact and their potential connection to mechanisms of cell survival/death represent a promising avenue that could provide essential insight. As a case in point, cadherin proteins, which mediate cell-cell interactions, can mediate Stat3 activation at high cell densities, and Stat3 activation in turn is tied to cell proliferation and survival [18]. Further exploration of these other pathways is vital to forming a more complete picture of the basis behind density-dependent chemoresistance.

In vivo/clinical relevance of cancer cell density-dependent chemoresistance

Special attention must be given to the translational relevance of *in vitro* density-dependent chemoresistance research. There is a significant potential of translating these findings to an *in vivo* context, which would undoubtedly yield stronger implications of this research for treating cancer in clinical settings. *In vivo* experiments would allow for the characterization of density-dependent chemoresistance in tumors and whether it operates on similar principles to the phenomenon observed *in vitro*. Regarding this study's findings involving autophagy and its connection to density-dependent chemoresistance, it would be useful to deter-

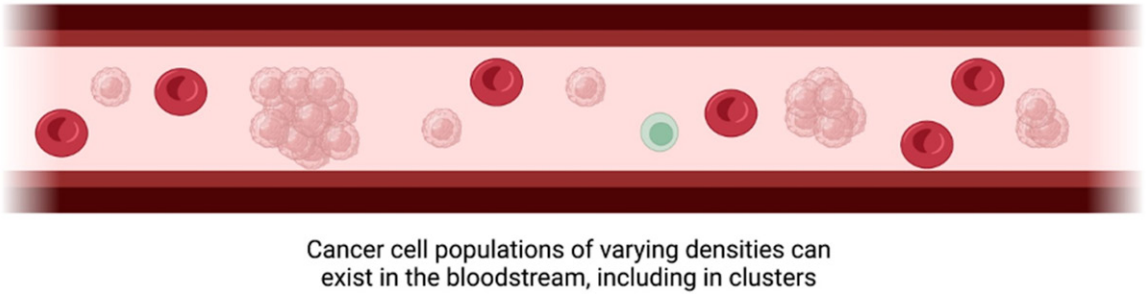

Figure 7. An illustration of the applicability of density-dependent chemoresistance to *in vivo* and clinical models. Within the bloodstream, cancer cells (shown in light red), can exist in multiple different densities, ranging from single cells to clusters. Leveraging density-dependent chemoresistance in order to develop strategies to target these cell populations of varying densities may be beneficial in clearing out cancer cells from the bloodstream.

mine how, if at all, the observed trends in autophagic activity at varying cell densities change in an *in vivo* context. Additionally, assessing whether targeting autophagy *in vivo* would improve the efficacy of chemotherapeutic treatments at varying tumor densities could open new avenues for anticancer clinical research efforts, particularly in the context of tackling chemotherapy resistance in tumors.

There are yet other dimensions to how density-dependent chemoresistance analyses can be translated to a clinical context. These include the problems of minimal residual disease and adjuvant chemotherapy. As mentioned earlier, most anticancer therapeutic regimens begin with cytoreductive surgery [19, 20]. Unfortunately, in many cases, the cytoreductive surgery is not guaranteed to completely clear the patient of cancer, which is why cytoreductive surgery is generally followed by adjuvant chemotherapy and/or radiation therapy [20]. Moreover, cancer cells may persist even after this round of adjuvant chemotherapy. Minimum residual disease is a term for cancer cells that remain in the body following a course of treatment, and is generally considered a marker for recurrent cancer. This is because the populations of cells that characterize minimal residual disease are generally so small that they do not cause any symptoms and are able to evade traditional cancer detection techniques. What makes these small cell populations such important aspects of anticancer therapeutic efforts is that cell growth can lead to the development of treatment-resistant tumors, and thus detecting and eliminating minimal residual disease as soon as possible is favorable for patient prognosis. Fortunately, recent advances have led to the use of such techniques as digital PCR (ddPCR), next-gen sequencing (NGS), and circulating tumor DNA (ctDNA) analysis to detect minimal residual disease [21]. With regard to treating these cell populations, it is proposed that the principle of density-dependent chemoresistance would be instrumental in devising strategies to model and clear minimal residual disease before it develops into the sort of therapy-resistant tumor that so often proves fatal to patients. Such strategies could include modulating the concentration/delivery method of the adjuvant chemotherapy based on the density of the detected cell populations, administering autophagy-inhibiting/apoptosis-inducing drugs along with the chemotherapy of interest, among others.

Another dimension of how the principle of density-dependent chemoresistance could be useful for clinical settings is the treatment of cancer cells in the bloodstream, often referred to as circulating tumor cells (CTCs). This is especially relevant in metastatic cancers, in which cancer cells have intravasated into the circulatory system and are traveling to other sites and organs in the body. Throughout the bloodstream, CTC populations can exist in a variety of cell densities, ranging from single cells to clusters of CTCs, called CTC microemboli (**Figure 7**). As a result, modeling and treating these CTC populations must necessarily take density-dependent chemoresistance into account, as challenging the chemotherapeutic resistance of dense populations, such as the aforementioned microemboli, to chemotherapy may involve some of the strategies previously discussed in this study [22].

Implications of the IC50-Seeding Density Slope (ISDS)

Lastly, in proposing a novel, standardized measurement for chemosensitivity in cancer cells, our findings address a major shortcoming in the field of drug response analysis, the importance of which has been articulated before. Haibe-Kains *et al*., in their analysis of the discrepancies in results between two major pharmacogenomic studies, contend that there are fundamental problems with how pharmaceutical response is currently assessed, and as a result any predictive models based on these assessments are unreliable. The authors specifically note how gene expression analysis, once seen as a notorious source of "noisy" and inconsistent data, has been standardized to the point where current experiments in the area are producing high quality, reproducible expression profiles [23]. In comparison, the lack of a similar consistency in drug phenotype response results is alarming. To that end, Hatzis *et al*. argue for the community-wide implementation of a standardized assay for measuring chemosensitivity in cancer cells, which would enable scientific endeavors that incorporate chemosensitivity analyses to reach their full potential. In particular, Hatzis *et al*. posit that the fact that cell culture conditions such as seeding density could affect drug responsiveness only renders the need for an international standard of chemosensitivity assays even greater. Moreover, increasing the reproducibility of experimental results is another major driving factor for the standardization of drug-response measurement methodologies [24]. As such, the ISDS, by considering the natural tendency of cancer cells to exhibit density-dependent chemoresistance, represents a concrete step toward that goal of standardized chemosensitivity measurements.

Conclusion

Our findings provide a detailed characterization of the phenomenon of density-dependent chemoresistance in cancer cells *in vitro*, demonstrating how seeding density can influence the viability response of multiple cell lines to different chemotherapeutic agents, how seeding density can modulate the efficacy of chemotherapy-induced cell death, and how a cancer cell's extracellular environment can play a role in influencing its susceptibility to chemotherapeutic treatment. We provide a method (IC50-Seeding Density Slope; ISDS) for incorporating cancer cell seeding density into chemosensitivity analysis. Furthermore, this study presents the first in-depth characterization of autophagy as it relates to density-dependent chemoresistance. By suggesting a link between autophagic flux and density-dependent chemoresistance, this study sheds light on a potential mechanism for how cancer cells could acquire increased resistance to chemotherapeutic agents and provides insight into strategies to increase the efficacy of anti-cancer treatment regimes.

Disclosure of conflict of interest

None.

Address correspondence to: Wafik S El-Deiry, Legorreta Cancer Center at Brown University, The Warren Alpert Medical School of Brown University, Providence, RI, USA. E-mail: wafik@brown.edu

References

[1] Ianevski A, He L, Aittokallio T and Tang J. SynergyFinder: a web application for analyzing drug combination dose-response matrix data. Bioinformatics 2017; 33: 2413-2415.

[2] He Y, Zhu Q, Chen M, Huang Q, Wang W, Li Q, Huang Y and Di W. The changing 50% inhibitory concentration (IC50) of cisplatin: a pilot study on the artifacts of the MTT assay and the precise measurement of density-dependent chemoresistance in ovarian cancer. Oncotarget 2016; 7: 70803-70821.

[3] Wu H, Ding Z, Hu D, Sun F, Dai C, Xie J and Hu X. Central role of lactic acidosis in cancer cell resistance to glucose deprivation-induced cell death. J Pathol 2012; 227: 189-199.

[4] Provencher DM, Lounis H, Champoux L, Tetrault M, Manderson EN, Wang JC, Eydoux P, Savoie R, Tonin PN and Mes-Masson AM. Characterization of four novel epithelial ovarian cancer cell lines. In Vitro Cell Dev Biol Anim 2000; 36: 357-361.

[5] Sahin I, Zhang S, Navaraj A, Zhou L, Dizon D, Safran H and El-Deiry WS. AMG-232 sensitizes high MDM2-expressing tumor cells to T-cell-mediated killing. Cell Death Discov 2020; 6: 57.

[6] Yadav B, Wennerberg K, Aittokallio T and Tang J. Searching for drug synergy in complex dose-response landscapes using an interaction po-

tency model. Comput Struct Biotechnol J 2015; 13: 504-513.
[7] Liu WJ, Ye L, Huang WF, Guo LJ, Xu ZG, Wu HL, Yang C and Liu HF. p62 links the autophagy pathway and the ubiqutin-proteasome system upon ubiquitinated protein degradation. Cell Mol Biol Lett 2016; 21: 29.
[8] Radha G and Raghavan SC. BCL2: a promising cancer therapeutic target. Biochim Biophys Acta Rev Cancer 2017; 1868: 309-314.
[9] Bjorkoy G, Lamark T, Brech A, Outzen H, Perander M, Overvatn A, Stenmark H and Johansen T. p62/SQSTM1 forms protein aggregates degraded by autophagy and has a protective effect on huntingtin-induced cell death. J Cell Biol 2005; 171: 603-614.
[10] Morsi RZ, Hage-Sleiman R, Kobeissy H and Dbaibo G. Noxa: role in cancer pathogenesis and treatment. Curr Cancer Drug Targets 2018; 18: 914-928.
[11] Liu Z, Ding Y, Ye N, Wild C, Chen H and Zhou J. Direct activation of bax protein for cancer therapy. Med Res Rev 2016; 36: 313-341.
[12] di Pietro A, Koster R, Boersma-van Eck W, Dam WA, Mulder NH, Gietema JA, de Vries EG and de Jong S. Pro- and anti-apoptotic effects of p53 in cisplatin-treated human testicular cancer are cell context-dependent. Cell Cycle 2012; 11: 4552-4562.
[13] Chipuk JE, Kuwana T, Bouchier-Hayes L, Droin NM, Newmeyer DD, Schuler M and Green DR. Direct activation of Bax by p53 mediates mitochondrial membrane permeabilization and apoptosis. Science 2004; 303: 1010-1014.
[14] Safa AR. Roles of c-FLIP in apoptosis, necroptosis, and autophagy. J Carcinog Mutagen 2013; Suppl 6: 003.
[15] Trajkovic K, Valdez C, Ysselstein D and Krainc D. Fluctuations in cell density alter protein markers of multiple cellular compartments, confounding experimental outcomes. PLoS One 2019; 14: e0211727.
[16] Balduini W, Carloni S and Buonocore G. Autophagy in hypoxia-ischemia induced brain injury. J Matern Fetal Neonatal Med 2012; 25 Suppl 1: 30-34.
[17] Hosseinpour-Moghaddam K, Caraglia M and Sahebkar A. Autophagy induction by trehalose: molecular mechanisms and therapeutic impacts. J Cell Physiol 2018; 233: 6524-6543.
[18] von Manstein V and Groner B. Tumor cell resistance against targeted therapeutics: the density of cultured glioma tumor cells enhances Stat3 activity and offers protection against the tyrosine kinase inhibitor canertinib. Medchemcomm 2016; 8: 96-102.
[19] Luqmani YA. Mechanisms of drug resistance in cancer chemotherapy. Med Princ Pract 2005; 14 Suppl 1: 35-48.
[20] Galaal K, Al Moundhri M, Bryant A, Lopes AD and Lawrie TA. Adjuvant chemotherapy for advanced endometrial cancer. Cochrane Database Syst Rev 2014; 2014: CD010681.
[21] Peng Y, Mei W, Ma K and Zeng C. Circulating tumor DNA and minimal residual disease (MRD) in solid tumors: current horizons and future perspectives. Front Oncol 2021; 11: 763790.
[22] Puleri DF, Balogh P and Randles A. Computational models of cancer cell transport through the microcirculation. Biomech Model Mechanobiol 2021; 20: 1209-1230.
[23] Haibe-Kains B, El-Hachem N, Birkbak NJ, Jin AC, Beck AH, Aerts HJ and Quackenbush J. Inconsistency in large pharmacogenomic studies. Nature 2013; 504: 389-393.
[24] Hatzis C, Bedard PL, Birkbak NJ, Beck AH, Aerts HJ, Stem DF, Shi L, Clarke R, Quackenbush J and Haibe-Kains B. Enhancing reproducibility in cancer drug screening: how do we move forward? Cancer Res 2014; 74: 4016-4023.